buildings

MDPI

Article

Evaluation of Interlayer Reinforcement Effectiveness in Road Pavement Rehabilitation Using FEM Modeling and Fracture Mechanics Analysis

Arianna Antoniazzi, Gianluca Ravizzoni, Cecilia Schiavone, Maurizio Crispino and Emanuele Toraldo *

Department of Civil and Environmental Engineering, Politecnico di Milano, 20133 Milano, Italy; arianna.antoniazzi@polimi.it (A.A.); gianluca.ravizzoni@mail.polimi.it (G.R.); cecilia.schiavone@mail.polimi.it (C.S.); maurizio.crispino@polimi.it (M.C.)
* Correspondence: emanuele.toraldo@polimi.it

Abstract: In this paper, the effectiveness of reinforcements for flexible pavements is evaluated through an analysis of reflective cracking. Different stiffness and thickness reinforcements are considered for the rehabilitation of an already cracked pavement. The effect of the reinforcement is assessed from two different perspectives: (i) the ability to reduce stresses in the rehabilitated pavement layers, and (ii) the capacity to mitigate the crack propagation from deeper layers. A finite element model (FEM) is adopted to study the stress and strain state of the pavement layers. The pavement model has been properly validated, transitioning from a simply supported beam scheme to an elastic multilayer model. In addition, to represent crack propagation, fracture evolution is analyzed using Linear Elastic Fracture Mechanics (LEFMs) and Paris' law. The effect of different reinforcements on the pavement is then simulated. The results show that the reinforcement performance is strictly dependent on the interlayer thickness and stiffness. In particular, high stiffness reinforcements (geomembranes) show increasing effectiveness with stiffness, both in terms of reflective cracking and stress reduction. Conversely, low stiffness reinforcements (SAMIs) show a variable trend with the stiffness modulus. In fact, extremely low stiffness is effective in slowing down crack propagation but is detrimental to the wearing course's stress condition. However, as the stiffness increases, the likelihood of cracking in the wearing course decreases, though only a small beneficial effect is registered for crack propagation in the base layer.

Keywords: pavement cracking; pavement reinforcement; SAMI; geomembrane; fracture mechanics; finite element modeling; elastic multilayer model

Citation: Antoniazzi, A.; Ravizzoni, G.; Schiavone, C.; Crispino, M.; Toraldo, E. Evaluation of Interlayer Reinforcement Effectiveness in Road Pavement Rehabilitation Using FEM Modeling and Fracture Mechanics Analysis. *Buildings* **2024**, *14*, 2264. https://doi.org/10.3390/buildings14082264

Academic Editor: Huayang Yu

Received: 24 June 2024
Revised: 10 July 2024
Accepted: 19 July 2024
Published: 23 July 2024

1. Introduction

Fatigue cracking is one of the most common distress mechanisms in asphalt pavements. It consists of the initiation and propagation of cracks due to the repeated loading of the pavement [1]. The fracture severity and speed of propagation depend on various intrinsic and extrinsic parameters of hot mix asphalt pavement, such as layer thickness, mechanical properties, applied load, and temperature [2]. Cracked pavement causes the loss of regularity, friction, and comfort for vehicles, with significant safety implications.

One possible intervention to slow down reflective cracking is the implementation of reinforcement layers. To place the reinforcement layer on an initially cracked pavement, it is necessary to partially mill the pavement so that the final level of the pavement is not changed. An interlayer of variable thickness is then placed, and a final asphalt overlay is applied to restore the pavement surface characteristics. The effectiveness of the reinforcement depends on the cracking extension in the original pavement, the thickness and stiffness of the reinforcement, the adhesion of the reinforcement to the adjacent layers, and the accuracy of the execution. This paper focuses mainly on the interlayer reinforcement properties to define the optimal solution in terms of reinforcement thickness and stiffness.

Until now, several reinforcement materials have been considered for applications, but a generic approach aimed at comparing different alternatives has not yet been developed. In fact, the objective of this paper is to define a range of possible effective reinforcement solutions, in terms of thickness and stiffness, that could be obtained by adopting various materials available on the market.

2. Literature Review

The fatigue resistance of pavements depends on a combination of factors; therefore, machine learning and predictive methods have been used to describe it [3].

Various techniques can be adopted to prevent crack initiation [4] or to delay crack propagation [5]. Some methods even involve the adoption of recycled materials [6].

In particular, to delay fatigue cracking propagation, different reinforcement interventions could be implemented. The process mainly consists of milling part of the surface course to place a reinforcement interlayer, over which an overlay is applied. A widely used method consists of placing a geocomposite interlayer between the existing pavement and a new asphalt overlay. The effectiveness of the geocomposite in delaying crack initiation and propagation has been evaluated through laboratory tests, showing that material properties play a crucial role [7]. For instance, the suitability of the mechanical properties of reinforcing materials could be assessed for both natural and synthetic textiles [8]. It should be noted that the effect of geosynthetics in delaying crack initiation and propagation is usually evaluated by laboratory tests, which do not take into account a previously cracked pavement [9]. Moreover, laboratory tests conducted to characterize fatigue resistance are affected by great dispersion and require a large sample size [10].

The Stress Absorbing Membrane Interlayer (SAMI) could also be implemented as interlayers. Various studies in the literature have analyzed the effectiveness of SAMIs through laboratory tests designed to simulate fatigue cracking through accelerated loading tests [11]. The effectiveness of SAMIs might depend on various boundary conditions, and it was shown that their introduction is not always beneficial to the road pavement. In particular, the benefits of the SAMI depend on its thickness and the shear stiffness of the interlayer, especially when applied to a cracked pavement [12,13]. Moreover, depending on the temperature, the effect of the SAMI could vary, and when dealing with visco-elastic materials, such as asphalt pavements, a change in temperature results in a change in stiffness. This confirms the importance of considering both reinforcement thickness and stiffness as study variables.

SAMIs are low stiffness interlayers that are able to absorb stress due to their deformability. A Finite Element Analysis, which was used to evaluate SAMIs, revealed that low stiffness is necessary, but extremely low stiffness could lead to undesirable effects, such as excessive strain in the overlay [14].

In addition, SAMIs that employ innovative materials, such as a fiber reinforced SAMI [15] and asphalt rubber SAMI [16], have also been considered.

Bonding efficiency is another important aspect of interlayer reinforcement. In fact, a defect in interlayer bonding could compromise the effectiveness of the reinforcement [17,18]. Researchers investigated the feasibility of applying geocomposites to a milled surface and showed that they can be successfully applied if properly implemented [19]. It was demonstrated that bonding properties depend on the reinforcement system type [20]. Moreover, the adoption of innovative materials (such as a basalt fiber mesh geotextile [21]) to improve adhesion has been taken into account.

Finite Elements Models (FEMs) have been adopted in the literature to describe crack propagation by means of Paris' law [22]. This method involves an energetic approach to describe fatigue cracking [23] based on the introduction of a Stress Intensity Factor (SIF) and the J-integral [24].

3. Research Objectives

In this study, the effectiveness of the reinforcement is evaluated according to the state of the art. In particular, as interlayer thickness and stiffness are essential characteristics, different values for these variables have been taken into account. To simulate the effect on crack propagation and stress condition in the pavement layers, a FEM method is adopted. The simulations consider an already cracked pavement as the initial condition, representing a more realistic situation for reinforcement implementation. In fact, crack initiation occurs at a localized defect and the number of load cycles inducing initiation is strictly dependent on the specific defect and is thus influenced by randomness [25]. However, the crack propagation trend depends on the overall pavement layer properties. Therefore, the focus of this study is to describe and simulate the crack propagation phase. In detail, crack propagation is simulated in accordance with Paris' law, which, based on the literature, is the most widely adopted approach to date.

In addition, the unreinforced pavement condition is also considered for crack propagation simulations. This allows the performance of the specific reinforcement type to be evaluated by comparing it with the zero-intervention solution. As a result, a set of appropriate reinforcement characteristics could be determined.

Specifically, the effectiveness of each type of reinforcement is assessed on the basis of the following criteria: (i) the ability to limit the stress condition in the asphalt overlay and prevent it from cracking, and (ii) the ability to slow down and delay the propagation of cracks in the initially cracked pavement. In fact, the cracking of the overlay would again compromise the surface properties of the pavement in terms of friction and therefore safety.

4. Materials and Methods

The purpose of this study is to assess the effectiveness of asphalt pavement reinforcement in counteracting reflective cracking. It is assumed that the rehabilitation intervention is carried out on an initially cracked pavement to limit the negative impact on user safety.

4.1. Pavement Rehabilitation and Reinforcement Layer

Road pavement rehabilitation involves the partial milling of the cracked pavement layers, the application of a reinforcement interlayer, and a final asphalt overlay to restore the surface characteristics. In particular, various reinforcement interlayer typologies have been taken into account in terms of stiffness and thickness. To evaluate the effectiveness of different types of reinforcement, it is necessary to simulate crack propagation scenarios in pavements without and with reinforcement. By comparing the results for the different reinforcements, the most effective solutions in terms of thickness and stiffness can be identified. In particular, the pavement layouts without reinforcement and with reinforcement are shown in Figure 1a and Figure 1b, respectively.

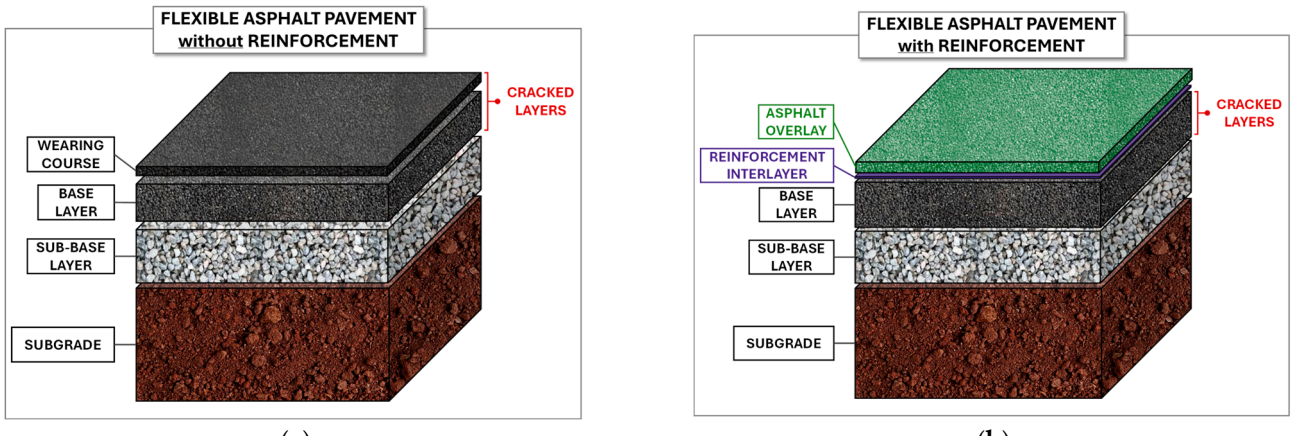

Figure 1. Analyzed pavement scheme: (**a**) without reinforcement; (**b**) with reinforcement.

There are different types of reinforcement interlayers in terms of material properties, stiffness, and operating principle. In this study, different interlayer typologies are considered regarding stiffness and thickness. In particular, by assuming a reasonable stiffness of 8000 MPa (at 20 °C and 10 Hz load frequency [26]) for the asphalt overlay, the following two categories of reinforcement have been identified.

- Low stiffness reinforcements refer to reinforcements characterized by a modulus of elasticity less than 8000 MPa. This stiffness range is usually associated with the Stress Absorbing Membrane Interlayer (SAMI). Thanks to their low stiffness and high deformability, these layers can absorb stresses and dissipate energy through vertical and horizontal deformation. The SAMI consists of a modified bituminous emulsion covered with a washed and crushed aggregate, forming a diaphragm that distributes the stresses and limits the propagation of cracks from the lower layers of the pavement.
- High stiffness reinforcements refer to reinforcements characterized by a modulus of elasticity greater than 8000 MPa. This reinforcement stiffness can be associated with geomembranes, which are layers of polymer modified bitumen and glass fiber reinforcements, characterized by a waterproofing function [27]. To ensure adhesion between layers, the geomembrane is composed of a three-layer system consisting of a self-adhesive bituminous lower layer, a glass fiber grid middle layer, and a bituminous upper layer with a thermo-adhesive surface.

For the simulations, different values of the elastic modulus are considered for low and high stiffness reinforcements, as shown in Table 1.

Table 1. Reinforcement elastic modules for low stiffness and high stiffness reinforcements.

Reinforcement Stiffness—Elastic Modulus [MPa]	
Low Stiffness Reinforcements -SAMI-	**High Stiffness Reinforcements -Geomembranes-**
400; 500; 600; 700; 800; 900; 1000; 1500; 2000; 3000; 4000; 5000.	10,000; 50,000; 100,000; 200,000.

4.2. Fracture Mechanics

The reflective cracking phenomenon on the pavement is typical of fatigue cracking under repeated load cycles [28,29]. In this study, crack propagation is analyzed by employing Linear Elastic Fracture Mechanics (LEFMs). This assumption is valid for linear elastic material properties. For visco-elastic materials, such as asphalt pavement, specific adjustments should be considered to adapt the LEFMs, as detailed below.

Crack propagation in a pavement can follow two typical paths: bottom-up [30] and top-down [31]. Bottom-up crack propagation occurs when the first crack appears at the bottom of the bonded layers and then propagates upwards, while top-down propagation starts at the surface layer and propagates downwards. Bottom-up propagation is considered for the present analysis, as it is the most common initiation condition caused by tensile stress at the lower surface of the base layer. To describe crack propagation, fracture mechanics should be considered. LEFMs divide the phenomenon into three stages: (i) crack initiation, (ii) crack propagation, and (iii) system failure. In addition, crack propagation may follow a different trend if a reinforcing layer is applied to an already cracked pavement. The crack propagation scheme for an unreinforced and a reinforced pavement is synthesized in Figure 2.

Relevant to this study, each stage of crack propagation is described in detail below.

1. Stage 1: Crack initiation. The crack initiation phase consists of two steps: an initial microcrack and a subsequent macrocrack, corresponding to the formation of a visibly damaged zone. The initiation phase is characterized by the number of repeated load cycles (N_i) causing the appearance of the first damage state within the affected layer. The location of the crack initiation zone depends on the presence of a localized defect.

It is hypothesized that the first crack initiates at the base of the bonded layers and then propagates upwards (bottom-up fatigue cracking), as this crack initiation mechanism is the most common in fatigue cracking [30]. The loading condition causing the crack formation is assumed to be a tensile stress opening the crack, since it has been shown to be the most critical condition for the crack propagation stage as well (Stage 2) [32].

2. Stage 2: Crack propagation. Once the first crack has appeared, if the pavement continues to be cyclically loaded, the crack will continue to propagate. A plastic zone develops at the tip of the crack, the size of which increases as the crack grows [33]. If the plastic region is small enough to be contained within the elastic singularity region, the Stress Intensity Factor (SIF) can be adopted to describe the stress field around the defect [34]. The SIF, represented by the variable K, can be adopted to estimate the fracture dimension (a) during its propagation. The SIF depends on the geometric and loading conditions and can be expressed in general terms for different loading modes by Equation (1).

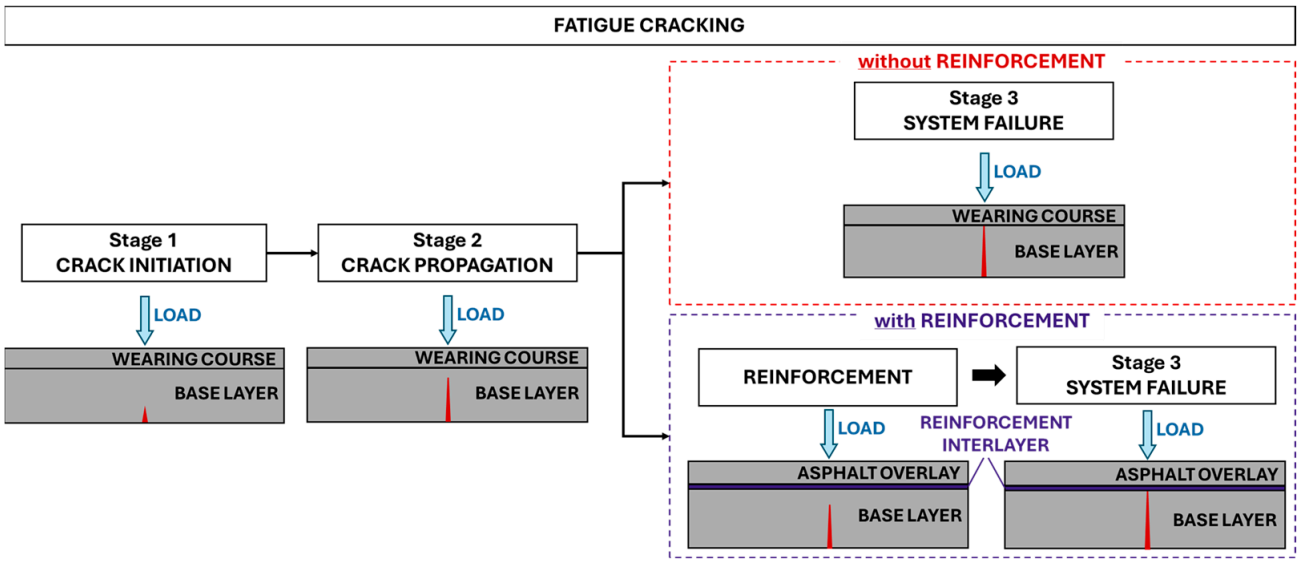

Figure 2. Crack propagation scheme for a non-reinforced and a reinforced pavement.

$$K = Y\sigma\sqrt{\pi a} \tag{1}$$

where σ is the applied stress, a is the crack size, and Y is an adimensional shape factor depending on the geometry and loading mode. To define the SIF, an energetic approach based on the J-integral is adopted. The J-integral is the energy parameter describing the concentration of stress over an area, as given by Equation (2).

$$J = -\frac{dU}{dA} \tag{2}$$

where U is the potential energy, and A is the fracture area. For visco-elastic materials such as asphalt pavement, the J-integral is expressed by Equation (3), through which the SIF is obtained, as expressed in Equation (4).

$$J = \frac{K^2(1-\nu^2)}{E_R} \tag{3}$$

$$K = \sqrt{\frac{E_R \cdot J}{(1-\nu^2)}} \tag{4}$$

where E_R is the reference stiffness modulus for the material, and ν is the Poisson's coefficient. The crack growth rate is a function of the change in the SIF (ΔK). The relationship describing crack propagation is expressed by Equation (5):

$$\frac{da}{dN} = f(\Delta K,\ R) \tag{5}$$

where a is the fracture dimension, N is the number of loading cycles, da/dN is the crack growth per load cycle, ΔK is the change in the SIF, and R is the fracture resistance of the material. Equations (6) and (7) can be adopted for determining the aforementioned parameters.

$$\mathrm{R} = \frac{K_{min}}{K_{max}} \tag{6}$$

$$\Delta K = K_{max} - K_{min} \tag{7}$$

By means of the relationship described in Equation (5), it is possible to estimate the fatigue life of the pavement, which refers to the number of load cycles that will bring the pavement to failure. The number of cycles to failure is calculated as the number of cycles required to propagate the crack from an initial height (a_0) to a final height (a_f), as expressed by Equation (8).

$$N = \int_{a_0}^{a_f} \frac{da}{f(\Delta K,\ R)} \tag{8}$$

In the crack propagation phase, the evolution essentially depends on the material properties. Indeed, the literature has shown that it is possible to characterize the trend of the defect propagation rate as a function of the K parameter using an exponential law that can be linearized in the logarithmic plane. The exponential law describing this trend is known as Paris' law and is expressed in Equation (9), where A and n are parameters characterizing the material.

$$\frac{da}{dN} = A(\Delta K)^n \tag{9}$$

In particular, n is assumed to be equal to 3.4 [35,36], while A is determined through Molenaar theory [37], as shown in Equation (10). This approach allows one to account for the visco-elastic properties of the analyzed material.

$$\log A = 4.389 - 2.52\ \log(E_r \cdot \sigma_t \cdot n) \tag{10}$$

where σ_t is the tensile strength of the material, which is assumed to be equal to 1.8 MPa.

3. Stage 3: System failure. System failure corresponds to the loss of the safety and operability of the road surface. In the case of a reinforced pavement, system failure is reached when the crack has propagated through the full thickness of the base layer reaching the reinforcement layer. For consistency, the system failure for a non-reinforced pavement is assumed to occur when the crack propagates through the entire base layer.

4.3. Method Validation

To validate the method adopted for the solution, an elementary model to describe the pavement is initially considered, namely a single-layer beam. The aim of validation is to confirm the ability of the software considered (COMSOL Multiphysics, and Abaqus) to describe the pavement behavior in terms of the following:

1. Stress trend, which should be consistent with the stress results from the de Saint Venant theory;
2. Crack propagation, which must be in accordance with the results based on Paris' law.

In particular, the validation is performed on a single-layer beam in the absence of a crack for the stress condition and in the presence of a crack for the crack propagation case. Moreover, the following hypotheses have been considered:

- Linear elastic material is assumed to describe asphalt behavior (reasonable assumption in the case of fatigue behavior with a high number of load cycles [38]); the material properties are therefore expressed in terms of the Young's modulus ($E = 8000$ MPa) and Poisson's coefficient ($\nu = 0.3$);
- Plane deformation state ($\varepsilon_x \neq 0, \varepsilon_y \neq 0, \varepsilon_z = 0$);
- Beam dimensions (length L = 500 mm and height h = 50 mm) are assumed to comply with the slender beam condition ($L/h \geq 8$), so that de Saint Venant's theory can be applied;
- A three-point loading condition is needed, with a load of 120 N distributed over an area of 10 mm (distributed load of 12 N/mm).

For the cracked beam simulation scenario, different crack dimensions (a) are assumed for the two software programs:

- For COMSOL Multiphysics, a variable crack height from 2.5 mm to 30 mm with 0.5 mm increments is considered;
- For Abaqus, crack heights of 5, 10, 15, 20, and 25 mm are considered.

Therefore, the single-layer beam scheme considered for stress validation is illustrated in Figure 3a, while the adopted configuration for crack propagation validation is represented in Figure 3b.

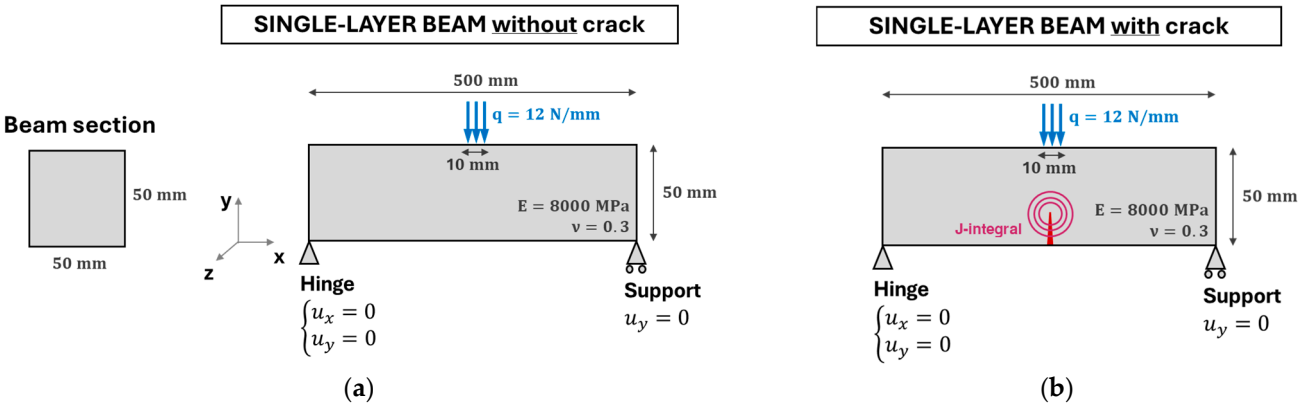

Figure 3. Single-layer beam scheme considered for model validation: (**a**) non-cracked single-layer beam for stress condition validation; (**b**) cracked single-layer beam for crack propagation validation.

4.3.1. Stress Condition

The validation of the stress condition is performed on the single-layer beam without a crack (Figure 3a). In fact, the stress results obtained from the software are compared with those obtained by de Saint Venant's theory. The stresses are calculated at the beam mid-point at various heights. However, as these stresses are influenced by local effects due to the presence of the load at the mid-point, stresses are also calculated at 200 mm from this point. Considering the trend of stresses corresponding to a section slightly shifted from the centerline (at 200 mm), where the concentrated load is applied allows for the effect of stress concentration to be isolated.

The graphical representation of the stresses at the beam centerline (Figure 4a) and 200 mm from the centerline (Figure 4b) shows that there is an almost perfect correspondence between the software and de Saint Venant's theory, except for localized effects caused by the load application. It can be seen that the middle section is affected by stress concentration effects due to the presence of the load, while the section 200 mm away shows an almost perfect correspondence between the software and de Saint Venant's theory. In fact, the stresses assume the pattern of the typical butterfly diagram.

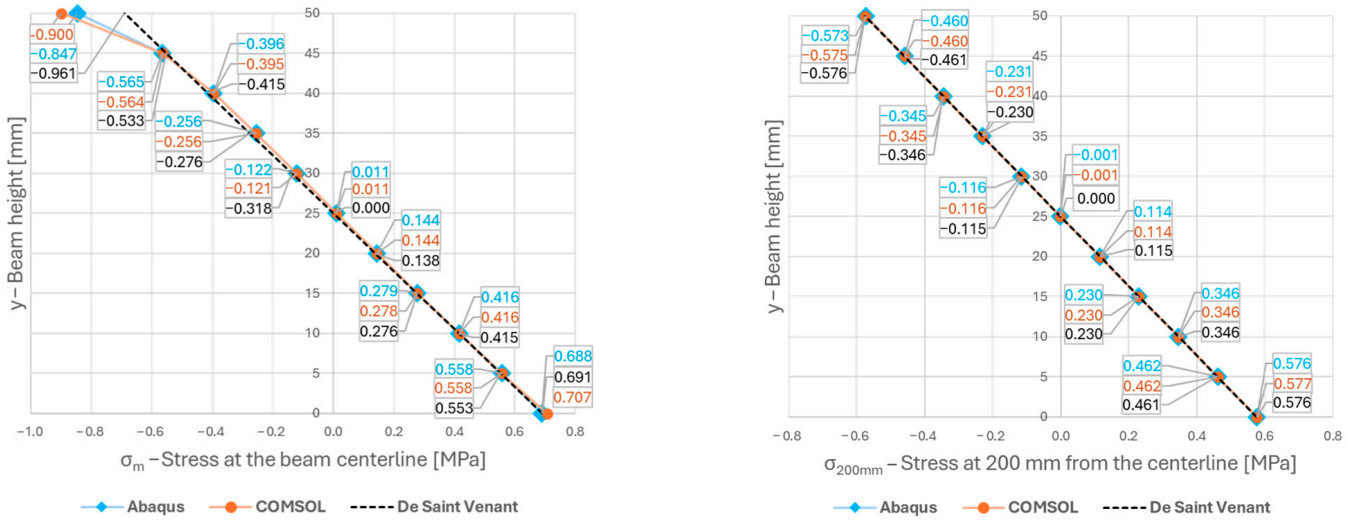

(**a**) (**b**)

Figure 4. Comparison of stress diagram in single-layer beam obtained with de Saint Venant theory and software: (**a**) at the beam centerline; (**b**) at 200 mm from the beam centerline.

4.3.2. Crack Propagation

The validation of the crack propagation is performed on the single-layer beam with the crack (Figure 3b). The software results are compared in terms of the Stress Intensity Factor (SIF) with the literature equations for the three-point bending test. In particular, the formulations of Anderson [33] and Carpinteri [39], described by Equations (11) and (12), respectively, are considered.

$$K = \frac{Q \cdot L}{h^{\frac{3}{2}} \cdot B} \cdot g\left(\frac{a}{h}\right) = \frac{Q \cdot L}{h^{\frac{3}{2}} \cdot B} \cdot \frac{3\sqrt{\frac{a}{h}}}{2 + \left(1 + 2 \cdot \frac{a}{h}\right) \cdot \left(1 - \frac{a}{h}\right)^{\frac{3}{2}}} \cdot \left[1.99 - \frac{a}{h} \cdot \left(1 - \frac{a}{h}\right) \cdot \left(2.15 - 3.93 \cdot \frac{a}{h} + 2.7 \cdot \frac{a}{h}^2\right)\right] \quad (11)$$

$$K = \frac{Q \cdot L}{h^{\frac{3}{2}} \cdot B} \cdot f\left(\frac{a}{h}\right) = \frac{Q \cdot L}{h^{\frac{3}{2}} \cdot B} \cdot 2.9 \cdot \left(\frac{a}{h}\right)^{\frac{1}{2}} - 4.6 \cdot \left(\frac{a}{h}\right)^{\frac{3}{2}} + 21.8 \cdot \left(\frac{a}{h}\right)^{\frac{5}{2}} - 37.6 \cdot \left(\frac{a}{h}\right)^{\frac{7}{2}} + 38.7 \cdot \left(\frac{a}{h}\right)^{\frac{9}{2}} \quad (12)$$

where Q is the concentrated load, L is the beam length, h is the beam height, B is the beam thickness, and $\frac{a}{h}$ is the ratio between the crack dimension and the beam height.

The results in terms of the SIF for different crack dimensions are synthesized in Table 2. It can be noted that the SIF shows a good correspondence between the software and literature equations.

Table 2. Comparison of the SIF obtained with the literature equations and software for different crack dimensions.

Crack Dimension	Stress Intensity Factor—K [N/m$^{1.5}$]			
a [mm]	Abaqus	COMSOL	Anderson	Carpinteri
5	91,444	90,577	90,906	89,071
10	129,826	129,317	126,101	125,430
15	169,746	168,887	163,277	163,446
20	220,866	218,773	212,711	212,629
25	291,328	291,290	285,769	286,028

The validation process confirmed the reliability of using both software programs to represent the stress condition and crack propagation. Therefore, only *COMSOL Multiphysics* is referred to in the following, as it allows for the easier modeling of the crack dimension. In particular, the crack is modeled with a variable height ranging from 2.5 mm to 30 mm with 0.5 mm increments.

4.4. Two-Layer System

Once the feasibility of adopting the software has been validated, the assumed model is refined to better represent the actual on-site condition of the pavement. Therefore, a two-layer beam is considered, with the top layer representing the wearing course and the bottom layer representing the base layer. It is assumed that there is perfect adhesion between the two layers. This condition is proven to be achieved in properly constructed pavements [19]. The graphical representation of the two-layer beam is shown in Figure 5. This pavement configuration allows for the investigation of the effect of different fracture dimensions on the stress condition and crack propagation of the two-layer system. Therefore, simulations for the two-layer beam can be extrapolated to the behavior of a non-reinforced pavement.

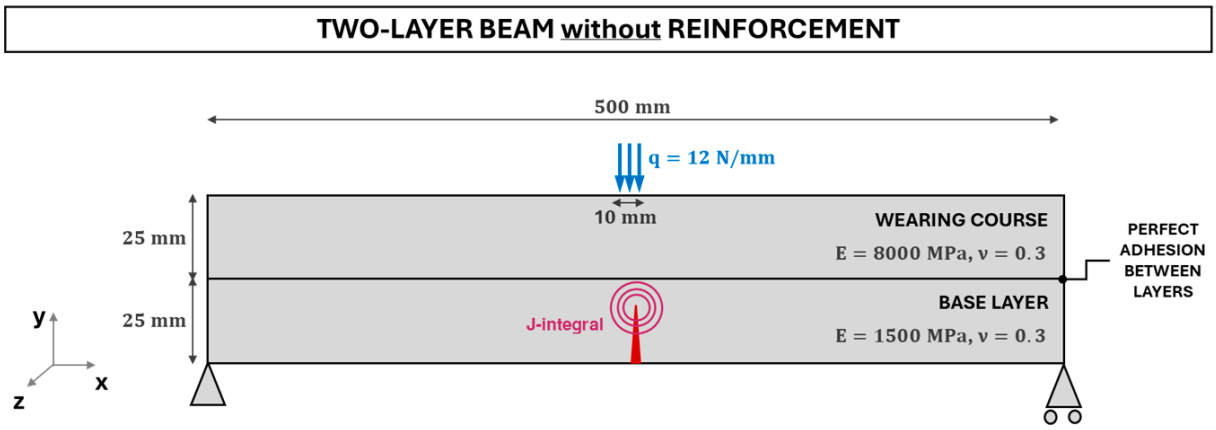

Figure 5. Non-reinforced pavement represented by a two-layer beam scheme.

The following results obtained from the software simulations are analyzed.

1. σ_x: stress along the x-direction calculated at the beam centerline for the entire beam height. Based on Figure 6, it can be noted that when considering increasing crack dimensions (a), an increasing stress trend is registered along the beam centerline. In addition, the maximum tensile stress is recorded in correspondence with the crack tip. Moreover, larger crack heights increase the stress in the wearing course, increasing the likelihood of crack initiation. If the crack extends through the entire base layer (a = 25 mm), the stress in the bottom layer is null and the stress in the top layer is maximized.
2. The J-integral and SIF for different crack dimensions and different radii of the circular integration area (r). A different J-integral will be calculated according to the selected circular radius for the integration area, as shown in Figure 7a. In particular, the value of the J-integral depends on the radius of the circular integration area (r) when the integration surface intersects the boundary between the lower and upper layers. Consequently, a specific SIF is obtained, as illustrated in Figure 7b.
3. N_{nr}: the number of load cycles to failure without reinforcement, where failure is reached when the crack propagates through the entire base layer. The number of cycles leading to system failure is calculated as the cumulative number of load cycles for several increasing crack heights. Thus, according to results expressed in Figure 8, the total number of load cycles that will cause the system to fail without reinforcement is approximately $N_{nr} = 6.71 \cdot 10^8$.

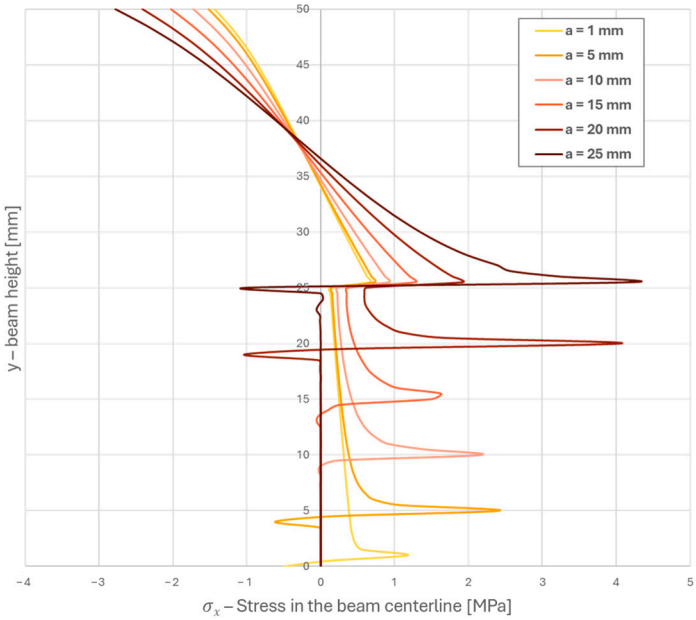

Figure 6. Stress at the beam centerline in a two-layer system for different crack dimensions (*a*).

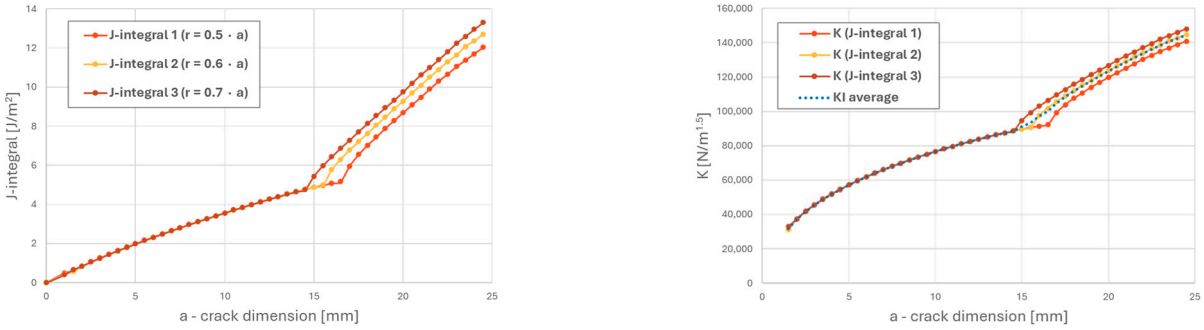

(**a**) (**b**)

Figure 7. Paris' law parameters in a two-layer system for different crack dimensions: (**a**) J-integral; (**b**) Stress Intensity Factor.

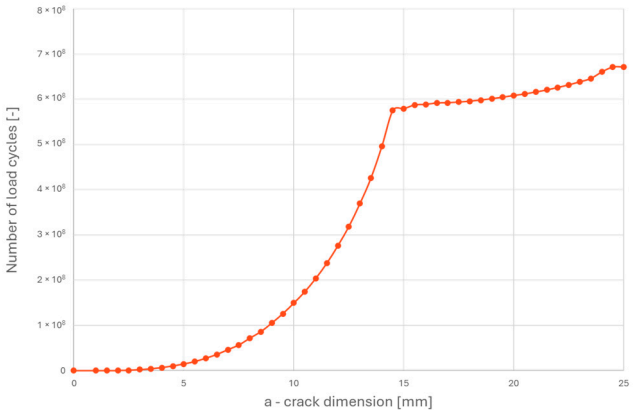

Figure 8. Cumulative load cycles leading the two-layer beam system to failure.

4.5. Three-Layer System

To simulate the effect of reinforcement with reference to the pavement scheme considered in Section 4.4, a three-layer beam is considered. Therefore, the pavement scheme

considered is shown in Figure 9. It should be noted that the effect of the reinforcement depends on its thickness and stiffness; thus, different simulations are performed for different reinforcement characteristics.

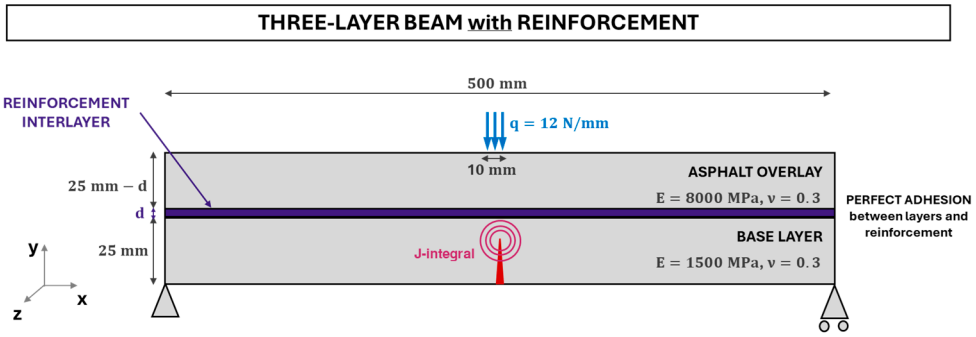

Figure 9. Reinforced pavement represented by a three-layer beam scheme.

Software simulations allow the number of cycles to failure to be determined for different reinforcement thicknesses and stiffnesses. In fact, the output data obtained from the software are the same as those considered in Section 4.4. However, for the reinforced pavement, the number of load cycles that bring the system to failure (crack propagation affecting the whole base layer) is expressed through the symbol N_r.

To determine the effect of the reinforcement on the wearing course, the maximum tensile stress recorded in the surface layer is evaluated for different reinforcement thicknesses and stiffnesses. The results reported in Figure 10 show that the tensile stress in the wearing course increases with the crack dimension. In fact, as the crack propagates from the deeper layer (base) upwards, the maximum stress in the surface layer increases. In addition, the positive effect of the reinforcement in containing the tensile stress in the wearing course is more pronounced at greater thicknesses and stiffnesses. When comparing two different reinforcing layer thicknesses, 0.15 mm (Figure 10a) and 2 mm (Figure 10b), for the same stiffness, the reinforcement proves to be more effective with a greater thickness. This means that the reinforcement layer should be sufficiently stiff and thick to prevent cracking in the wearing course.

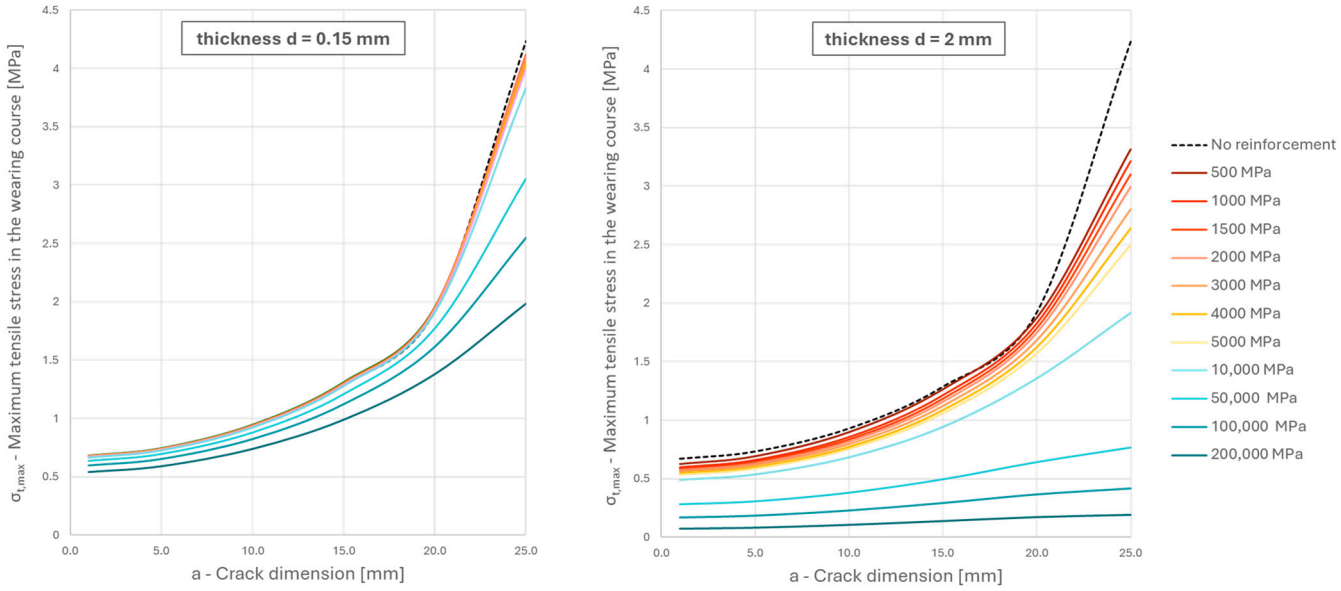

(**a**) (**b**)

Figure 10. Maximum tensile stress in the wearing course for increasing crack dimension: (**a**) for a reinforcement thickness d = 0.15 mm; (**b**) for a reinforcement thickness d = 2 mm.

Similarly, when comparing the effect of reinforcement for two different crack dimensions, 1 mm (Figure 11a) and 25 mm (Figure 11b), a combined effect of the layer thickness and stiffness is registered. In small crack dimensions, the effect of the reinforcement layer is significant only for high reinforcement stiffness (>8000 MPa). Conversely, for larger crack dimensions, the effect of reinforcement is noticeable even for lower stiffness layers when they have a sufficient thickness.

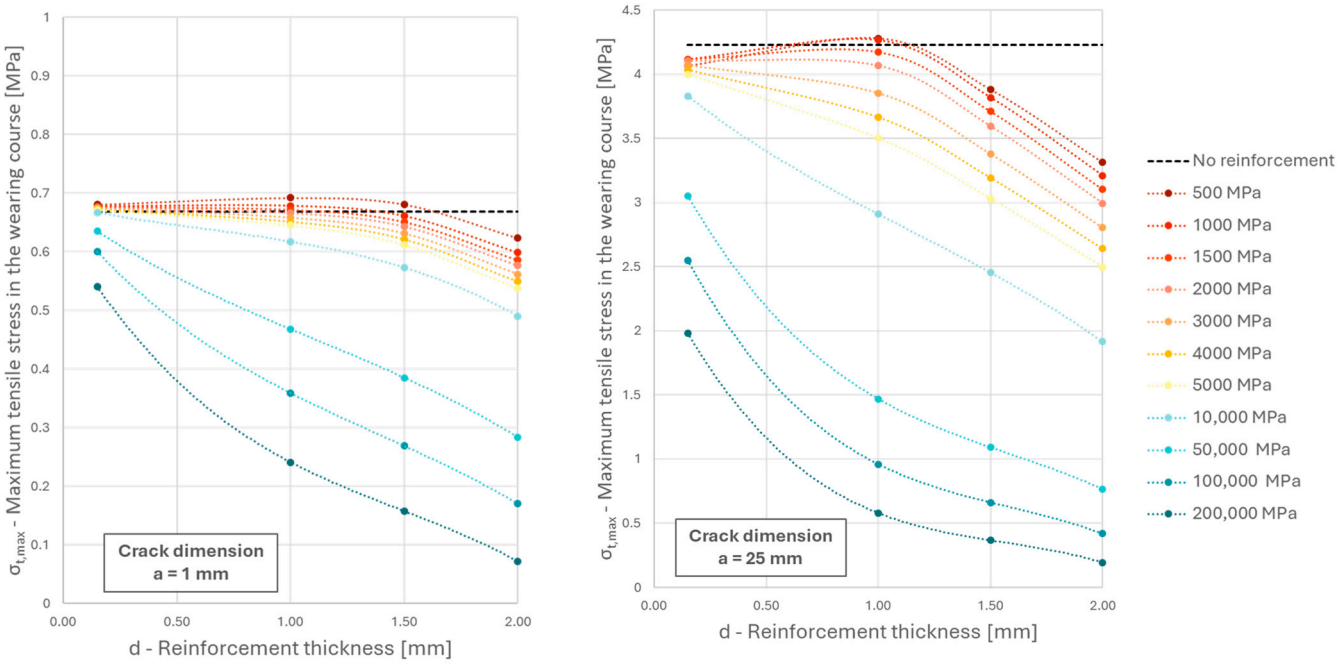

(**a**) (**b**)

Figure 11. Maximum tensile stress in the wearing course for increasing reinforcement thickness: (**a**) for a crack dimension a = 1 mm; (**b**) for a crack dimension a = 25 mm.

4.6. Reinforcement Performance

To evaluate the effect of the reinforcement layer on the base layer, crack propagation should be considered. In particular, the performance of the reinforcement is described in terms of the number of cycles to failure with and without reinforcement, through the following Equation (13):

$$\eta = \frac{N_r}{N_{nr}} = \frac{\int_0^H \cdot \frac{da}{(\Delta K_r)^n}}{\int_0^H \cdot \frac{da}{(\Delta K_{nr})^n}} \quad (13)$$

where η is the reinforcement performance, N_{nr} is the number of load cycles to failure without reinforcement, N_r is the number of load cycles to failure with reinforcement, ΔK_{nr} is the SIF for the non-reinforced pavement, and ΔK_r is the SIF for the reinforced pavement. Whenever the performance value is greater than one, the reinforcement has a positive effect on crack propagation in the base layer.

The results in terms of reinforcement performance for different thicknesses and stiffnesses are synthetized in Table 3.

Table 3. Reinforcement performance for different thicknesses and stiffnesses.

Reinforcement Thickness d [mm]	Reinforcement Performance—η [-]																
	Low Stiffness [MPa]												[MPa]	High Stiffness [MPa]			
	400	**500**	**600**	**700**	**800**	**900**	**1000**	**1500**	**2000**	**3000**	**4000**	**5000**	**8000**	**10,000**	**50,000**	**100,000**	**200,000**
0.15	0.85	0.87	0.88	0.89	0.90	0.90	0.91	0.92	0.93	0.95	0.96	0.97	1.00	1.01	2.04	3.40	34.67
1.00	4.41	1.74	1.19	0.99	0.90	0.85	0.82	0.77	0.76	0.78	0.82	0.86	1.00	1.11	6.90	82.85	632,942.53
1.50	1.50	1.11	0.95	0.87	0.82	0.79	0.76	0.72	0.71	0.73	0.77	0.82	1.00	1.16	17.86	1903.29	6,065,251.51
2.00	0.81	0.72	0.68	0.66	0.64	0.63	0.62	0.61	0.62	0.66	0.71	0.77	1.00	1.20	48.02	2659.01	35,576.08

The results show that high modulus reinforcements consistently exert a positive effect on crack propagation in the base layer due to their stiffening effect. Specifically, they offer increasingly significant benefits with a higher modulus and thickness. Conversely, low stiffness modulus reinforcements have no stiffening effect and, due to stress redistribution, increase the tensile stresses in the base layer and reduce the number of cycles to failure. In fact, for low stiffness reinforcements, the performance η is generally less than one, which represents a negative effect on crack propagation. The only low stiffness reinforcement configuration associated with a positive effect is for extremely low stiffness moduli (<700 MPa) and for intermediate thicknesses (d = 1 mm or d = 1.5 mm).

Figure 12 synthetizes the reinforcement performance at different stiffness levels, confirming that high modulus reinforcements always have a positive effect in delaying crack propagation, while low modulus reinforcements are mainly inefficient except at very low stiffness values.

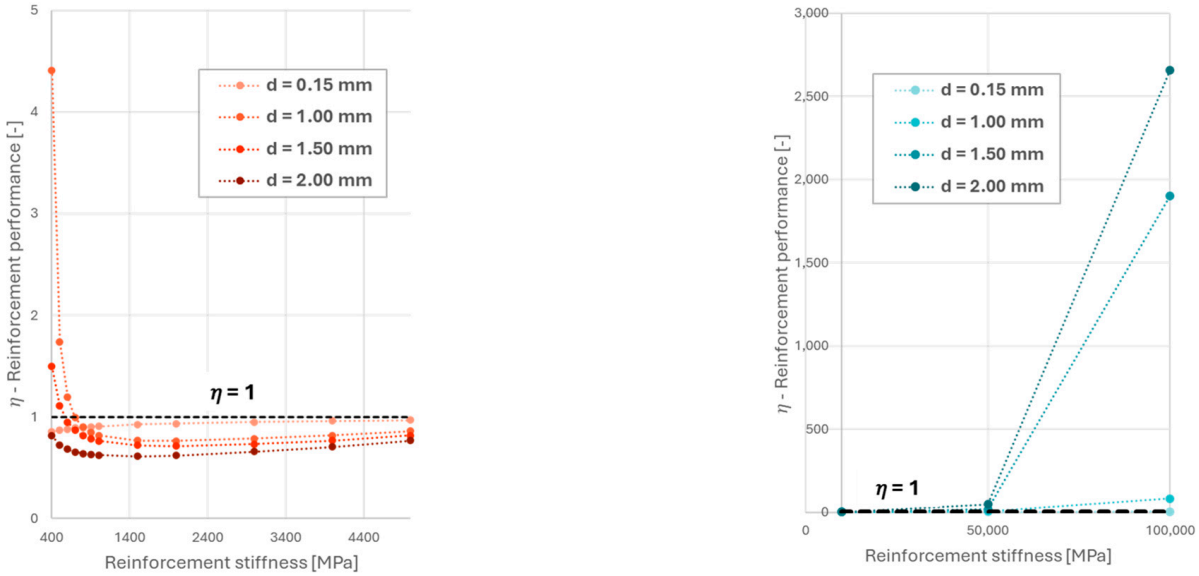

Figure 12. Reinforcement performance at different thicknesses and stiffnesses for: (**a**) low stiffness reinforcements; (**b**) high stiffness reinforcements.

4.7. Multilayer System

Once the main trends between reinforcement thickness/stiffness and its performance have been defined, a more realistic pavement configuration is simulated. In particular, a multilayer system representing an asphalt pavement is considered. Specifically, the asphalt bonded layers (wearing course and base) are placed on top of an unbonded layer (sub-base) laying on the subgrade. The specific pavement scheme without reinforcement and its relative material properties and boundary conditions is shown in Figure 13. In particular, the bottom of the subgrade is considered fixed (displacements are not allowed along both the x and y directions). Lateral boundaries of the multilayer system are represented as a trolley, which prohibits any movement along x and allows translations only along y. The interaction between the different layers is simulated according to two different schemes: (i) a condition of perfect adhesion is assumed at the interface between the bonded layers, i.e., total cooperation with the transfer of vertical stresses and the same horizontal deformations, and (ii) at the interface with at least one unbonded layer, the total absence of adhesion is assumed, with the layers being completely independent from the tensile-deformation point of view, thus eliminating the transfer of horizontal forces. To simulate reflecting cracking, a variable crack dimension between 0.1 mm and 170 mm in 0.5 mm increments is assumed so that for the maximum crack height, the entire base layer is cracked. For the purpose of finite element modeling, the mesh characteristics were determined. A structured triangular

mesh with a maximum dimension of 5 mm and densification near the fracture apex was assumed, as detailed in Figure 13.

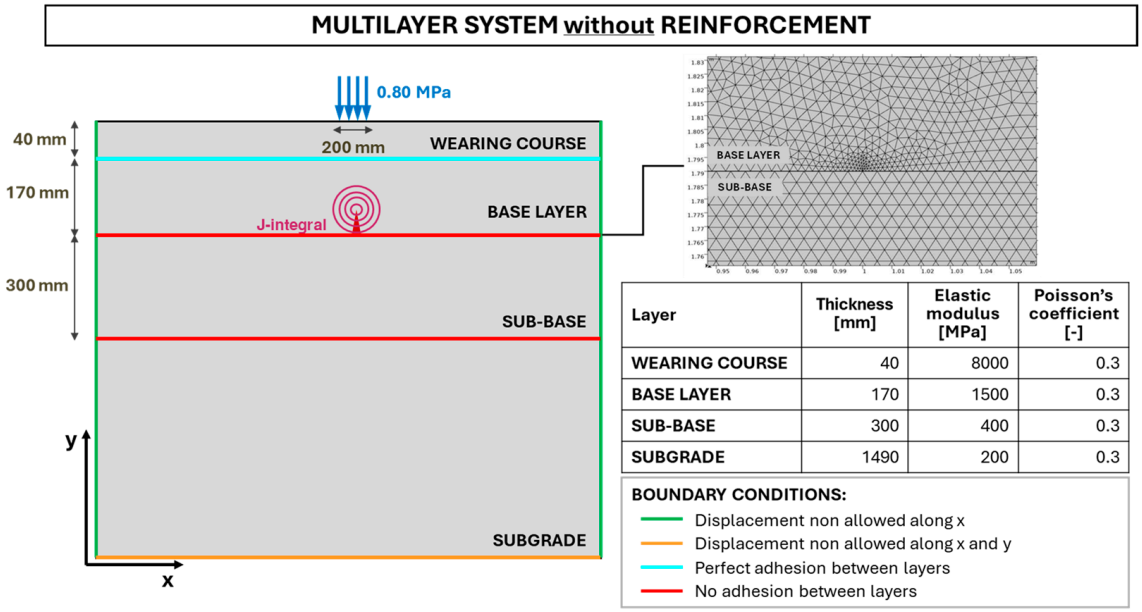

Layer	Thickness [mm]	Elastic modulus [MPa]	Poisson's coefficient [-]
WEARING COURSE	40	8000	0.3
BASE LAYER	170	1500	0.3
SUB-BASE	300	400	0.3
SUBGRADE	1490	200	0.3

Figure 13. Multilayer pavement scheme without reinforcement.

To calculate the J-integral, four different circular integration surfaces with an increasing radius r (10 mm, 20 mm, 30 mm, and 40 mm) are considered. The software, therefore, simulates the stress condition and crack propagation to failure.

Similarly, the reinforced pavement scheme is assumed, as shown in Figure 14. In this case, the software is used to run simulations for different reinforcement thicknesses and stiffnesses. It should be noted that for low stiffness reinforcements (SAMIs), a thickness of 5 mm is taken into account, while for high stiffness reinforcements (geomembranes), a thickness of 0.15 mm is considered. In particular, since the geomembrane is a three-layer system composed of two bituminous layers comprising a fiberglass grid, an equivalent thickness is taken into account. This allows for the consideration of the average reinforcement material properties for software simulation purposes.

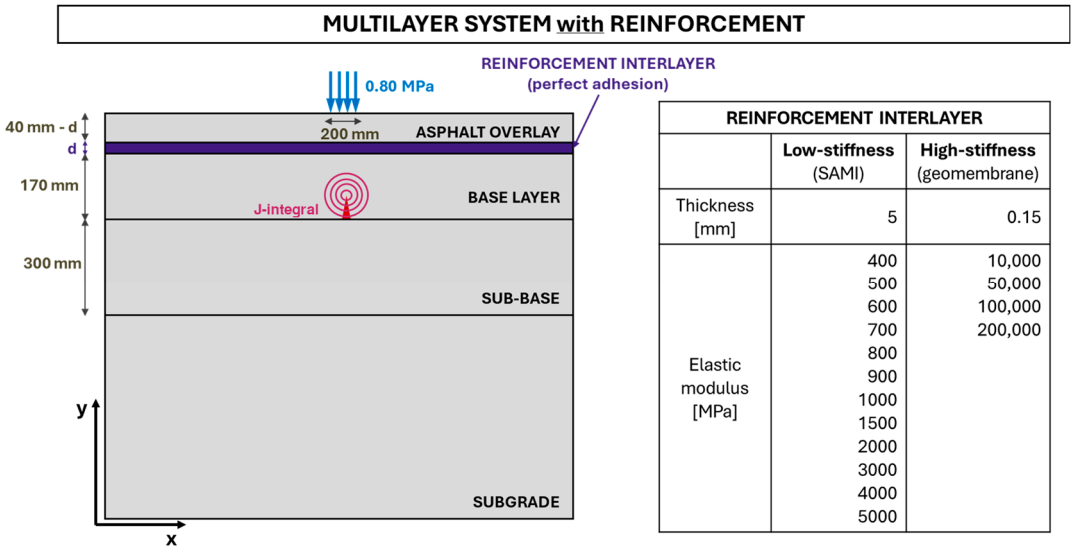

REINFORCEMENT INTERLAYER		
	Low-stiffness (SAMI)	High-stiffness (geomembrane)
Thickness [mm]	5	0.15
Elastic modulus [MPa]	400 500 600 700 800 900 1000 1500 2000 3000 4000 5000	10,000 50,000 100,000 200,000

Figure 14. Multilayer pavement scheme with reinforcement.

The thickness of the asphalt overlay depends on the thickness of the reinforcement, ensuring that the total thickness of reinforcement and overlay is equal to 40 mm. Regarding the elastic modulus, various values have been considered for both low and high stiffness reinforcements, as reported in Figure 14.

5. Results and Discussion

The effect of the reinforcement on the schematized pavement is evaluated by comparing the non-reinforced configuration (Figure 13) with the reinforced one (Figure 14). In particular, two aspects should be considered: the effect on the stress condition in the wearing course, and the crack propagation in the base layer. In fact, the reinforcement should be able to both prevent new cracking in the wearing course and delay crack propagation into a deeper layer of the pavement.

5.1. Reinforcement Effect on the Stress Condition of the Wearing Course

To evaluate the effectiveness of the reinforcement in preventing cracking in the wearing course, the maximum tensile stress is considered for various scenarios. In particular, the unreinforced pavement is compared with the reinforced pavement for various stiffness values.

5.1.1. Low Stiffness Modulus Reinforcements—SAMI

The results of the simulations in terms of the maximum tensile stress in the wearing course for low stiffness reinforcements are shown in Figure 15. It can be noted that low stiffness reinforcements (E < 8000 MPa) with a thickness of 5 mm are not always beneficial for preventing cracking in the wearing course. In fact, extremely low stiffness reinforcements (E < 700 MPa) induce a tensile stress in the wearing course that is even more critical compared to the unreinforced pavement. This phenomenon may be due to the presence of an interlayer contributing to the transfer of stresses from the lower cracked layers to the new asphalt overlay, overloading it. Only for fairly large cracks (a > 150 mm), which nearly affect the entire base layer, a slight positive effect of the reinforcement is observed. Conversely, stiffness values equal or greater than 700 MPa allow a positive effect to be achieved in the wearing course. In addition, the benefit is more pronounced for increasing stiffness. However, for the simulated scenarios, any reinforced pavement will still reach a fracture state if the crack extends to the full height of the deeper layers, as the tensile strength (1.80 MPa) is overcome.

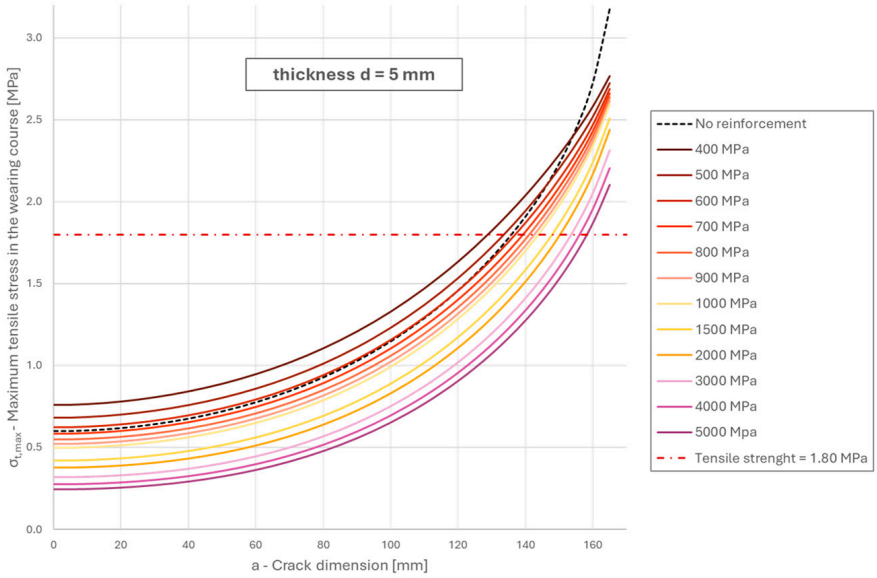

Figure 15. Maximum tensile stress in the wearing course for low stiffness reinforcements.

5.1.2. High Stiffness Modulus Reinforcements—Geomembranes

Regarding high stiffness reinforcements (E > 8000 MPa), a constant thickness of 0.15 mm is considered. As shown in Figure 16, high stiffness reinforcements are almost always effective in preventing cracking in the wearing course. In fact, even for a crack dimension of 170 mm affecting the entire base layer, the maximum tensile stress in the wearing course is below the tensile strength (equal to 1.8 MPa). The tensile strength is exceeded for a crack dimension of 170 mm only in the case of a reinforcement stiffness of 10,000 MPa, meaning that cracking will occur in the wearing course.

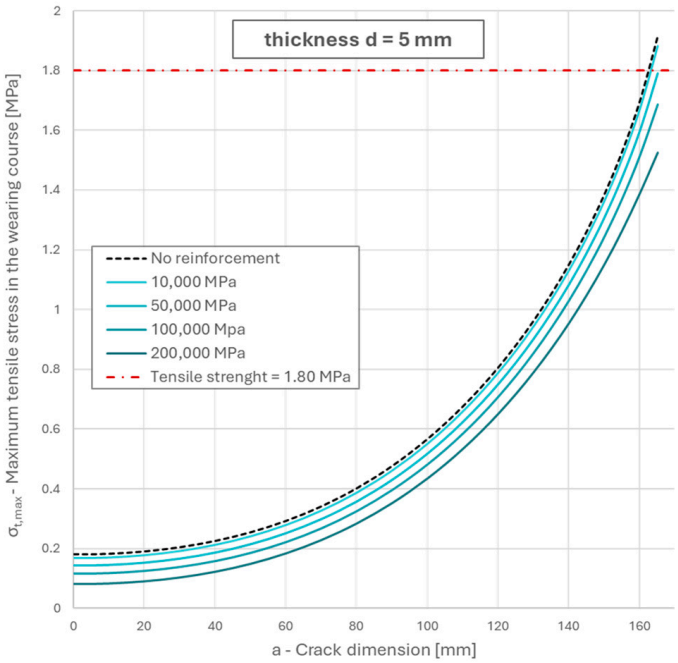

Figure 16. Maximum tensile stress in the wearing course for high stiffness reinforcements.

Therefore, high stiffness reinforcements with a modulus of elasticity greater or equal to 50,000 MPa are effective in preventing cracking in the surface layer. In addition, the maximum tensile stress in the wearing course is reduced as the stiffness of the reinforcement layer increases.

5.2. Reinforcement Effect on the Cracking State of the Base Layer

To evaluate the effectiveness of the reinforcement in delaying crack propagation in the base layer, the number of load cycles to failure are considered for various scenarios. Specifically, the unreinforced pavement is compared with the reinforced one for various stiffness values. Thus, the reinforcement performance (η) is computed according to Equation (13). Performance values greater than one express a positive effect of the reinforcement, as the number of cycles to failure is increased compared to the unreinforced pavement. Conversely, performance values lower than one indicate a detrimental effect of the reinforcement on crack propagation in the base layer.

5.2.1. Low Stiffness Modulus Reinforcements—SAMI

Performance values for low stiffness reinforcements are calculated by comparing the number of cycles to failure with no reinforcement and with 5 mm of reinforcement. The results presented in Figure 17 show that a beneficial effect is registered for a reinforcement stiffness of less than 900 MPa. In fact, for this condition, a performance value greater than one is obtained, meaning that the reinforcement can counteract crack propagation in the base layer. This means that low stiffness reinforcements, due to their high deformability, can slow down crack propagation. Conversely, as stiffness increases, the positive effect of

stress absorption is gradually reduced, so that for a modulus of elasticity between 900 MPa and 5000 MPa, the reinforcement is neither deformable enough to absorb stresses nor stiff enough to reinforce the deeper layers. As a result, the performance values are less than one and the reinforcement is not beneficial.

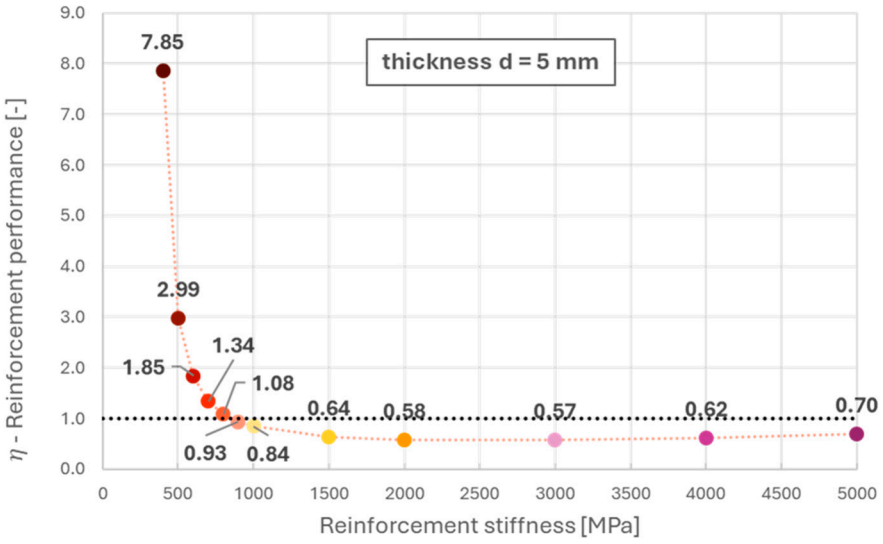

Figure 17. Reinforcement performance for low stiffness reinforcements.

5.2.2. High Stiffness Modulus Reinforcements—Geomembranes

Performance values for high stiffness reinforcements are calculated by comparing the number of cycles to failure with no reinforcement and with 0.15 mm of reinforcement. The results presented in Figure 18 show that a beneficial effect is always registered. In fact, for a modulus of elasticity greater or equal to 10,000 MPa, the performance values are always greater than one. This means that the number of cycles to failure is always increased compared to the unreinforced pavement. In the case of high stiffness reinforcements, the beneficial effect on the base layer in terms of crack propagation delay increases with stiffness.

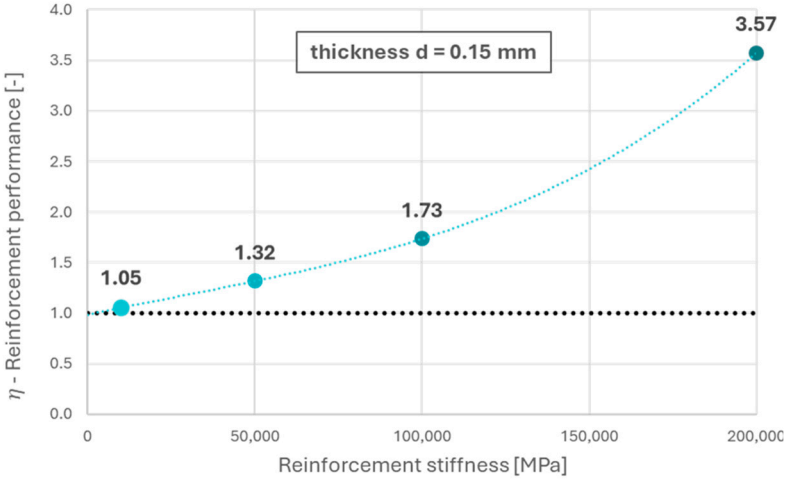

Figure 18. Reinforcement performance for high stiffness reinforcements.

6. Conclusions

This study aimed to evaluate the effectiveness of reinforcement interlayers in road pavement rehabilitation by mitigating fatigue cracking. Two types of interlayers were considered: (i) low stiffness reinforcements (SAMIs) and (ii) high stiffness reinforcements

(geomembranes). The benefits of reinforcement were evaluated based on the stress condition of the wearing course and the cracking state of the base layer.

The results showed that geomembranes always have a positive effect in terms of tensile stress in the wearing course. Moreover, interlayers with a very high stiffness (≥50,000 MPa) are effective in preventing cracking in the surface course, even with a fully cracked deeper course. In addition, geomembranes can delay crack propagation as the performance values are always greater than one. The performance increases with increasing stiffness, ranging from 1.05 (for 10,000 MPa reinforcement stiffness) to 3.57 (for 200,000 MPa reinforcement stiffness). For example, a 50,000 MPa geomembrane (0.15 mm thick) can increase the service life of a pavement by approximately 30%.

While geomembranes always have a positive effect, SAMIs do not always have a positive effect. In terms of tensile stress in the wearing course, a stiffening effect is required and a sufficiently high stiffnesses is necessary to have a positive effect on the existing pavement (≥700 MPa). In addition, the tensile strength in the wearing course is always exceeded for a totally cracked base layer, meaning that SAMIs are not fully effective in preventing cracking. In terms of crack propagation in the base layer, SAMIs only have a positive effect for sufficiently low stiffness (sufficiently deformable), showing performance values greater than one for reduced stiffness (≤800 MPa). Therefore, SAMIs present some critical issues related to the fact that they should be sufficiently deformable to delay crack propagation in the base layer, but stiff enough to prevent cracking in the wearing course.

In conclusion, geomembranes always have a positive effect both in delaying crack propagation in the deeper layers and in preventing cracking in the surface layer. On the contrary, SAMIs have a positive effect in reducing the probability of cracking in the wearing course for sufficiently high stiffnesses (≥700 MPa) and in retarding the propagation of cracks for sufficiently low stiffnesses (≤800 MPa). Thus, SAMIs could be effective for intermediate stiffnesses (700/800 MPa). However, the effect would be slightly positive and not comparable to that of geomembranes.

The results of this study, based on the simulation of pavement behavior, could be useful to plan an experimental analysis to confirm the results obtained, as the focus of a further agenda.

Author Contributions: Conceptualization, M.C.; methodology, E.T.; software, A.A.; validation, A.A.; formal analysis, A.A.; investigation, G.R. and C.S.; resources, G.R. and C.S.; data curation, G.R. and C.S.; writing—original draft preparation, A.A.; writing—review and editing, E.T.; visualization, A.A.; supervision, M.C. and E.T. All authors have read and agreed to the published version of the manuscript.

Funding: This research received no external funding.

Data Availability Statement: Dataset available on request from the authors.

Conflicts of Interest: The authors declare no conflicts of interest.

References

1. Walubita, L.F.; Simate, G.S.; Ofori-Abebresse, E.; Martin, A.E.; Lytton, R.L.; Sanabria, L.E. Mathematical formulation of HMA crack initiation and crack propagation models based on continuum fracture-mechanics and work-potential theory. *Int. J. Fatigue* **2012**, *40*, 112–119. [CrossRef]
2. Harne, V.R.; Tripathi, R.K.; Guzzarlapudi, S.D. Effect of extrinsic and intrinsic parameters on fatigue performance of hot mix asphalt mixtures: A review. *J. Build. Pathol. Rehabil.* **2024**, *9*, 53. [CrossRef]
3. Alnaqbi, A.J.; Zeiada, W.; Al-Khateeb, G.; Abttan, A.; Abuzwidah, M. Predictive models for flexible pavement fatigue cracking based on machine learning. *Transp. Eng.* **2024**, *16*, 100243. [CrossRef]
4. Rith, M.; Woo Lee, S. Evaluation of Asphalt Overlay Pretreatments against Reflective Crack Using Association Rule Mining. *J. Transp. Eng. Part B Pavements* **2021**, *147*, 04021042. [CrossRef]
5. Raheem, H.M.; Abduljabbar, A.S. Using Deferment Improvement Techniques to Mitigate Reflection Cracks in Composite Pavements. *AIP Conf. Proc.* **2023**, *2775*, 060016. [CrossRef]
6. Zvonarić, M.; Dimter, S. Prevention and remediation measures for reflective cracks in flexible pavements. *Gradjevinar* **2022**, *74*, 189–197. [CrossRef]

7. Asadi, S.; Shafabakhsh, G. Presenting a Statistical Model of Fatigue Prediction for the Effect of Loading Frequency on Reflective Cracks Propagation on Asphalt Layers Improved by Geosynthetics. *J. Rehabil. Civ. Eng.* **2024**, *12*, 18–33. [CrossRef]
8. Sudarsanan, N.; Mohapatra, S.R.; Karpurapu, R.; Amirthalingam, V. Use of Natural Geotextiles to Retard Reflection Cracking in Highway Pavements. *J. Mater. Civ. Eng.* **2018**, *30*, 04018036. [CrossRef]
9. Nejad, F.M.; Noory, A.; Toolabi, S.; Fallah, S. Effect of using geosynthetics on reflective crack prevention. *Int. J. Pavement Eng.* **2015**, *16*, 477–487. [CrossRef]
10. Sun, H. geng Development of an indoor test method for evaluating the anti-reflection crack performance of asphalt overlay. *Case Stud. Constr. Mater.* **2023**, *19*, e02241. [CrossRef]
11. Moses, O. Mechanical Behaviour of Stress Absorbing Membrane Interlayers. Ph.D. Thesis, The University of Nottingham, Nottingham, UK, 2012.
12. Ogundipe, O.M.; Thom, N.H.; Collop, A.C. Evaluation of performance of stress-absorbing membrane interlayer (SAMI) using accelerated pavement testing. *Int. J. Pavement Eng.* **2013**, *14*, 569–578. [CrossRef]
13. Ogundipe, O.M.; Thom, N.; Collop, A. Investigation of crack resistance potential of stress absorbing membrane interlayers (SAMIs) under traffic loading. *Constr. Build. Mater.* **2013**, *38*, 658–666. [CrossRef]
14. Ogundipe, O.M.; Thom, N.H.; Collop, A.C. Finite element analysis of overlay incorporating stress absorbing membrane interlayers against reflective cracking. *J. Mod. Transp.* **2014**, *22*, 104–111. [CrossRef]
15. Baek, C. Performance evaluation of fiber-reinforced, stress relief asphalt layers to suppress reflective cracks. *Appl. Sci.* **2020**, *10*, 7701. [CrossRef]
16. Zhang, K.; Zhang, Z.; Luo, Y. Material Composition Design and Anticracking Performance Evaluation of Asphalt Rubber Stress-Absorbing Membrane Interlayer (AR-SAMI). *Adv. Mater. Sci. Eng.* **2018**, *2018*, 8560604. [CrossRef]
17. Yuya, W.; Yasushi, T.; Futoshi, K.; Kazuhiro, W. Evaluation of the Effect of Interlayer Bonding Condition on the Deterioration of Asphalt Pavement. *Transp. Res. Rec.* **2023**, *2677*, 500–508. [CrossRef]
18. Sudarsanan, N.; Karpurapu, R.; Amrithalingam, V. Critical review on the bond strength of geosynthetic interlayer systems in asphalt overlays. *Jpn. Geotech. Soc. Spec. Publ.* **2015**, *2*, 2296–2301. [CrossRef]
19. Canestrari, F.; Cardone, F.; Gaudenzi, E.; Chiola, D.; Gasbarro, N.; Ferrotti, G. Interlayer bonding characterization of interfaces reinforced with geocomposites in field applications. *Geotext. Geomembr.* **2022**, *50*, 154–162. [CrossRef]
20. Raab, C.; Arraigada, M.; Partl, M.N.; Schiffmann, F. Cracking and interlayer bonding performance of reinforced asphalt pavements. *Eur. J. Environ. Civ. Eng.* **2017**, *21*, 14–26. [CrossRef]
21. Zhu, Z.; Xiao, P.; Kang, A.; Kou, C.; Wu, B.; Ren, Z. Innovative design of self-adhesive basalt fiber mesh geotextiles for enhanced pavement crack resistance. *Geotext. Geomembr.* **2023**, *52*, 368–382. [CrossRef]
22. Elseifi, M.A.; Baek, J.; Dhakal, N. Review of modelling crack initiation and propagation in flexible pavements using the finite element method. *Int. J. Pavement Eng.* **2018**, *19*, 251–263. [CrossRef]
23. Zhang, Z.; Roque, R.; Birgisson, B. Evaluation of laboratory-measured crack growth rate for asphalt mixtures. *Transp. Res. Rec.* **2001**, *1767*, 67–75. [CrossRef]
24. Luo, X.; Zhang, Y.; Lytton, R.L. Implementation of pseudo J-integral based Paris' law for fatigue cracking in asphalt mixtures and pavements. *Mater. Struct. Constr.* **2016**, *49*, 3713–3732. [CrossRef]
25. Santos, I.; Chupin, O.; Piau, J.M.; Marsac, P.; Hammoum, F. Modeling of fatigue cracking in asphalt materials based on the paris law with an initialization term-calibration from notched and unnotched specimens. *J. Test. Eval.* **2023**, *51*, 2132–2146. [CrossRef]
26. Brovelli, C.; Crispino, M.; Pais, J.; Pereira, P. Using polymers to improve the rutting resistance of asphalt concrete. *Constr. Build. Mater.* **2015**, *77*, 117–123. [CrossRef]
27. International Geosynthetics Society. Available online: https://www.geosyntheticssociety.org/educational-documents/geosynthetics-classification/ (accessed on 1 May 2024).
28. Chen, A.; Airey, G.D.; Thom, N.; Li, Y. Characterisation of fatigue damage in asphalt mixtures using X-ray computed tomography. *Road Mater. Pavement Des.* **2023**, *24*, 653–671. [CrossRef]
29. Si, C.; Cao, H.; Fan, T.; Jia, Y.; Wang, X.; Li, S.; Xu, Z.; Gu, J. Study on crack propagation behavior of bridge deck asphalt pavement. *Constr. Build. Mater.* **2024**, *425*, 136136. [CrossRef]
30. Zhang, J.; Zhang, J.; Cao, D.; Ding, Y.; Zhou, W. Mechanistic analysis of bottom-up crack in asphalt pavement using cohesive zone model. *Theor. Appl. Fract. Mech.* **2023**, *125*, 103904. [CrossRef]
31. Sun, L.; Wang, G.; Zhang, H.; Liu, L. Initiation and propagation of top-down cracking in asphalt pavement. *Appl. Sci.* **2018**, *8*, 774. [CrossRef]
32. Casey, D.B.; Collop, A.C.; Grenfell, J.R.; Airey, G.D. Stress Intensity Factors at the Tip of a Surface Initiated Crack Caused by Different Contact Pressure Distributions. *Procedia-Soc. Behav. Sci.* **2012**, *48*, 733–742. [CrossRef]
33. Ted, L. *Anderson Fracture Mechanics: Fundamentals and Applications*, 3rd ed.; CRC Press: Boca Raton, FL, USA, 2005; ISBN 9780429125676.
34. Irwin, G.R. Analysis of Stresses and Strains Near the End of a Crack Traversing a Plate. *J. Appl. Mech.* **1957**, *24*, 361–364. [CrossRef]
35. Elseifi, M. Performance Quantification of Interlayer Systems in Flexible Pavements Using Finite Element Analysis, Instrument Response, and Non Destructive Testing. Ph.D. Thesis, Virginia Tech, Blacksburg, VA, USA, 2003.
36. Ferraresi, F. Analisi Numerico-Sperimentale Sulla Resistenza a Fatica dei Conglomerati Bituminosi Rinforzati. Master's Thesis, Politecnico di Milano, Milan, Italy, 2010.

37. Francken, L.; Beuving, E.; Molenaar, A.A.A. *Reflective Cracking in Pavements: Design and Performance of Overlay Systems*; CRC Press: Boca Raton, FL, USA, 1996; Volume 1, p. 576.
38. Taliercio, A. Capitolo 7—Il Problema di Saint-Venant. In *Introduzione alla Meccanica dei Solidi*, 2nd ed.; Società Editrice Esculapio: Bologna, Italy, 2014.
39. Carpinteri, A. *Meccanica dei Materiali e della Frattura*; Pitagora Editrice: Bologna, Italy, 1992.